Crack initiation induced nanograins and facets of a titanium alloy with lamellar and equiaxed microstructure in very-high-cycle fatigue

Xiangnan Pan, Shouwen Xu, Alexander Nikitin, Andrey Shanyavskiy, Thierry Palin-Luc, Youshi Hong

Crack initiation induced nanograins and facets of a titanium alloy with lamellar and equiaxed microstructure in very-high-cycle fatigue

Xiangnan Pan [a], *Shouwen Xu* [a], *Alexander Nikitin* [b], *Andrey Shanyavskiy* [c], *Thierry Palin-Luc* [d,e], *Youshi Hong* [a,*]

[a] LNM, Institute of Mechanics, Chinese Academy of Sciences, Beijing 100190, China

[b] MAI – National Research University, 4, Volokolamskoe Hwy, A-80, GSP-3, Moscow 125993, Russia

[c] Aviation Register for the Russian Federation, Air. Sheremetevo-1, PO Box 54, Moscow Reg., Chimkinskiy State, 141426, Russia

[d] Univ. Bordeaux, CNRS, Bordeaux INP, I2M, UMR 5295, F-33400, Talence, France

[e] Arts et Metiers Institute of Technology, CNRS, Bordeaux INP, Hesam Universite, I2M, UMR 5295, F-33400 Talence, France

*Corresponding author: hongys@imech.ac.cn, Tel: +86-10-82543966, Fax: +86-10-62561284

Abstract

Fractographic and microstructure features in crack initiation region in very-high-cycle fatigue (VHCF) were characterized for an extruded titanium alloy VT3-1 under stress ratios R =−1 and 0.1. The material consists of lamellar and equiaxed microstructure. All specimens failed by internal crack initiation with rough area feature in VHCF. Within the rough area region, facets initiated from a big cluster of lamellar α at R = 0.1, and nanograin layers formed at some local areas underneath fracture surfaces due to insufficient contact of NCP (numerous cyclic pressing) process in the inhomogeneous microstructure at R = −1. Here, NCP mechanism still dominates the VHCF behavior of this titanium alloy under negative stress ratios, and facets dominate at R > 0.

Keywords: titanium alloy; crack initiation; facet; nanograin; fatigue; microstructure.

1. Introduction

Titanium alloys have been widely used in aeronautical engineering (e.g. gas turbines) due to their good mechanical properties [1]. In gas turbine industry, very-high-cycle fatigue (VHCF) has drawn substantial attention [2-5] since there is an increasing demand for the safe performance over 10^7 loading cycles. Crack initiation always plays a key role in VHCF as it consumes most of the total fatigue life beyond 95% [6]. For tension-tension fatigue, i.e. stress ratios $R > 0$, facets often appeared on the fracture surface as typical features of crack initiation in near α and α+β titanium alloys [7] that can be with equiaxed, bimodal, lamellar, or basketweave microstructure. When the equiaxed [8,9] or bimodal microstructure [10] experienced VHCF, there are usually several identifiable regions of crack initiation with rough area on the fatigue fractures. Nevertheless, no similar rough area morphology was observed in the cases of lamellar [11] or basketweave microstructure [12].

Within the rough area region, although facets prevail at $R = -1$ for a gradient equiaxed microstructure [13], facet formation also occurs at $R > 0$, and the amount of facets increases with stress ratio [14]. Traditionally, equiaxed α grains are considered as the defects to induce crack initiation in titanium alloys, and the α/β interfaces are regarded as the weak links if the volume fraction of equiaxed α is insufficient [15,16]. Thus, facets are related to the defects or weak links, which is a hint for revealing the fatigue crack initiation mechanism under positive R-values. As the stress ratio decreases, facet morphology becomes vague, indiscernible, and eventually vanishes at $R = -1$ for common titanium alloys.

In this paper, a titanium alloy with both equiaxed and lamellar microstructure is investigated to determine the fractographic and microstructure features at crack initiation region with rough area feature under negative and positive stress ratio. These results may help to understand the VHCF failure process in titanium alloys with different microstructures.

2. Material and methods

The studied material is an extruded titanium alloy, with the chemical composition (weight %) of 6.3 Al, 2.0 Mo, 1.25 Cr, 0.46 Fe, 0.32 Si, and balance Ti. Its mechanical properties under quasi-static monotonic tension along the extruded direction are [17]: ultimate tensile strength 1107 MPa, yield strength 1050 MPa, and elongation 13% at rupture. The as-received material is a round bar with a diameter of 10 mm (Fig. 1a).

According to the ultrasonic fatigue testing method [18], specimens were machined to the geometry (Fig. 1b) from the bars coaxially. One screw end with M5 for $R = -1$ and two screw ends for $R = 0.1$ are designed. Fatigue tests were conducted under axial cycling with the frequency of 20 ± 0.5 kHz at room temperature and in air. Fig. 1c presents the S-N data. Two specimens #1 ($R = -1$, $\sigma_m = 0$, $\sigma_a = 400$ MPa and $N_f = 2.84 \times 10^8$ cycles) and #2 ($R = 0.1$, $\sigma_m = 357$ MPa, $\sigma_a = 300$ MPa and $N_f = 2.24 \times 10^7$ cycles) representing VHCF with a negative and a positive stress ratio were selected for the detailed investigation.

Scanning electron microscopy (SEM) shows that the material is with both lamellar and equiaxed feature exhibiting the microstructure with significant difference in longitudinal (Fig. 1d) and vertical (Fig. 1e) directions of extrusion via JEOL JSM-IT300. More details were described in Ref. [19]. The crack initiation regions of specimens #1 and

#2 were carefully examined by optical microscopy (OM: ZY-HD4K), SEM/FIB (focused ion beam) dual system (FEI Helios Nanolab 600i) and transmission electron microscopy (TEM: FEI Talos F200X, FEI Tecnai G2 F20 S-Twin and FEI Tecnai G2 F30 S-Twin).

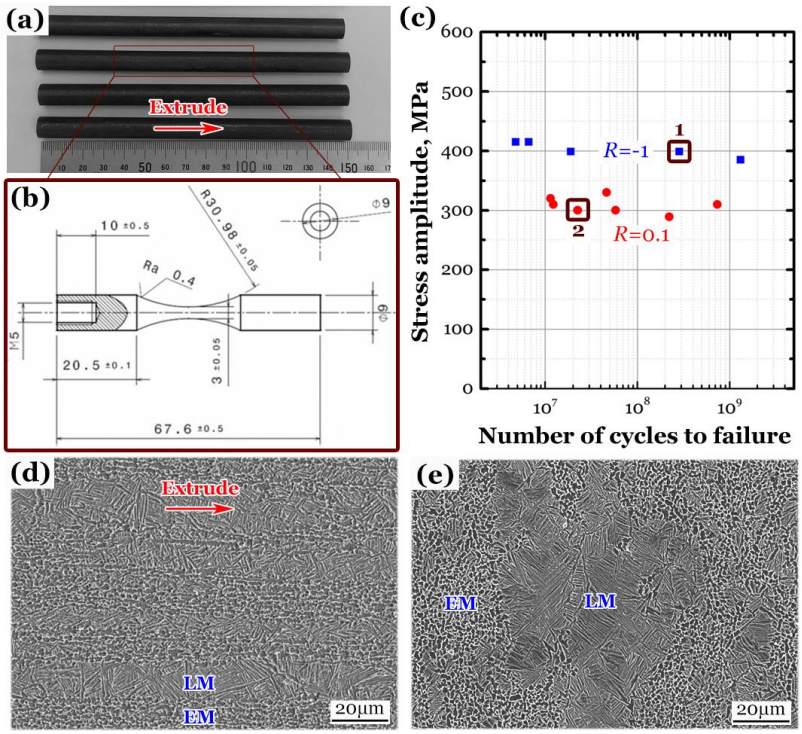

Fig. 1. (a) as-received round bars, (b) ultrasonic fatigue specimen (dimensions in mm), (c) S-N data and selected specimens #1 and #2, (d) microstructure of longitudinal section, and (e) microstructure of vertical section.

3. Results and discussion

As shown in the OM images of Fig. 2a and b, the specimens failed by internal crack initiation with rough area regions. For positive *R*-value (Fig. 2b), the rough area region is easier to be identified and optically darker than the negative case (Fig. 2a). Fig. 2c and d of SEM images demonstrate two typical rough area morphologies of crack initiation region in VHCF regime under $R = -1$ and 0.1. Fig. 2c exhibits radial ridges, grinding marks, and vague rings encircling the core region of rough area. In contrast, Fig. 2d presents the clear morphology of several large facets, as marked by the green arrows, which is intrinsically

related to the microstructure feature at the rough area region.

Subsequently, TEM samples 1 and 2 were extracted from the rough area region of crack initiation as the red bars indicated in Fig. 2c and d, which were prepared by FIB milling. The FIB location of sample 1 was arbitrarily chosen in the near center of the rough area region, and sample 2 was deliberately positioned at a large facet surface. Fig. 2e and f of TEM characterizations give the profile bright field morphologies and typical selected area electron diffraction patterns of the samples.

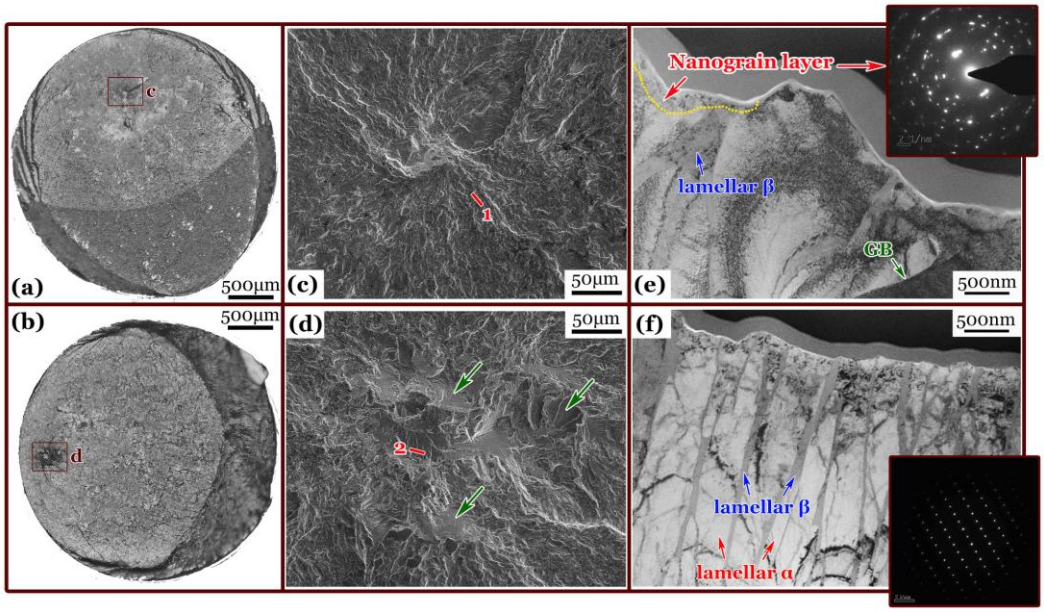

Fig. 2. Fracture surfaces of specimes #1 (R = −1, σ_m = 0, σ_a = 400 MPa and N_f = 2.84 × 10^8 cycles) and #2 (R = 0.1, σ_m = 357 MPa, σ_a = 300 MPa and N_f = 2.24 × 10^7 cycles) under OM (a,b). Crack initiation regions under SEM (c,d) for boxes in (a,b). (e,f) bright field images with selected area electron diffraction patterns for TEM samples 1 and 2 marked by red bars in (c,d). Green arrows in (d) indicating facets. GB: grain boundary.

For sample 1, there is a local nanograin layer underneath the fracture surface, and the microstructure is composed of lamellar β and irregular α grains with clear grain boundaries in the rest region. For sample 2, lamellar α and β are stacked and bonded to each other layer by layer with similar crystal orientation consisting of a lamellar microstructure colony.

This suggests that big facets are cracked from lamellar microstructure domains in the material. Detailed discussion about facets was described in Ref. [19].

Fig. 3 shows the TEM characterizations for sample 1. Fig. 3a of the bright field image demonstrates basically coarse-grained microstructure. Fig. 3b-e are four selected area electron diffraction patterns corresponding to the circular domains b-e with the size of 200 nm marked in Fig. 3a, which were representatives for tens of such selected area electron diffraction detections. Fig. 3b exhibits polycrystalline rings suggesting nanograins are smaller than 200 nm in the localized region of sample 1 (boxes f and g in Fig. 3a) and Fig. 3c-e present single crystalline spots. The nanograin layer was further examined by the comparison between the enlarged bright field and dark field images of Fig. 3f and g.

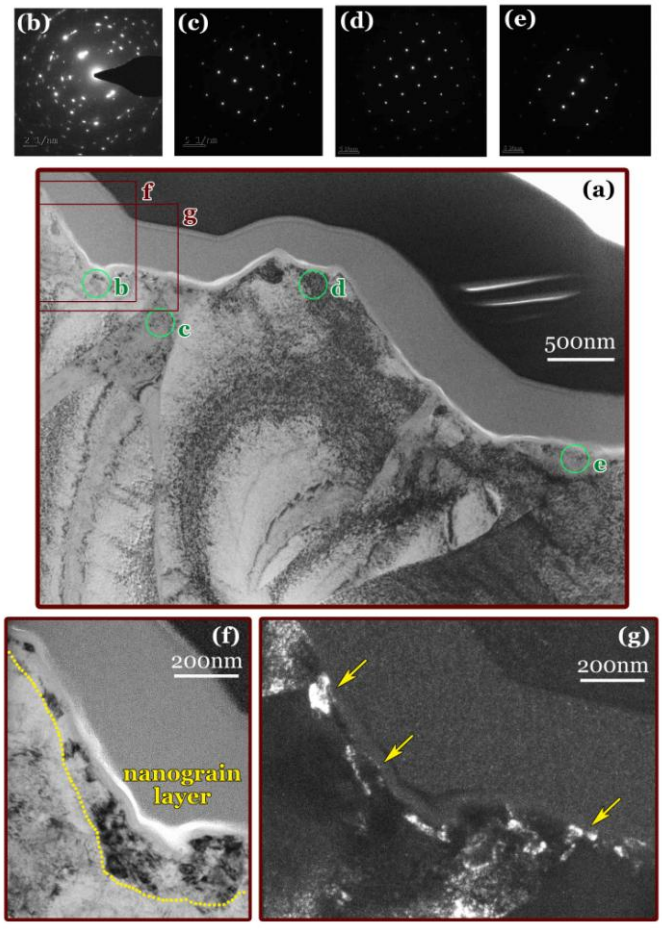

Fig. 3. TEM characterizations for sample 1, (a) bright field morphology, (b-e) selected area

electron diffraction patterns for circular domains in (a), enlarged bright field (f) and dark field (g) images for boxes in (a). Yellow arrows in (g) indicating nanograins.

It is seen that, nanograins can be regarded as a typical feature of crack initiation for the material with both lamellar and equiaxed microstructure in VHCF under a negative stress ratio ($R < 0$). Numerous cyclic pressing (NCP) [20] and local severe plastic deformation [21] are two common mechanisms for fatigue and fracture-induced nanograin formation. The presence of facets or nanograins is dependent on R-value. According to the NCP model, nanograin formation is attributed to the effects of repeated crack open and closure enduring VHCF. The repeated pressure of the crack lips in VHCF regime with negative R ratio is the driving force for nanograin formation.

4. Conclusions

In summary, different mechanisms for VHCF crack initiation under $R < 0$ and $R > 0$, i.e. tension-compression and tension-tension type loadings in titanium alloys, are clarified. For $R < 0$, the NCP process dominates the microstructure evolution in the rough area region owing to the compressive stress and crack closure. Thus, the NCP mechanism prevails not only in equiaxed microstructure and bimodal microstructure but also in lamellar microstructure. For $R > 0$, the VHCF crack initiation is not limited to the interior of equiaxed α grains or the interfaces between α and β phases, but depends on the size of grains, colonies or clusters with the same crystal orientation.

CRediT authorship contribution statement

X. Pan: conceptualization, methodology, investigation, analysis, visualization, writing-original draft, supervision, resources. S. Xu: investigation. A. Nikitin: resources. A. Shanyavskiy: resources, supervision. T. Palin-Luc: resources, supervision. Y. Hong:

supervision, writing-review and editing.

Data availability

Data will be made available on request.

Acknowledgments

This work was financially supported by the National Natural Science Foundation of China (11932020).

References

[1] J. Williams, E. Starke, Acta Mater. 51 (2003) 5775.

[2] A. Atrens, W. Hoffelner, T. Duerig, J. Allison, Scripta Metall. 17 (1983) 601.

[3] A. Shanyavskiy, I. Nikitin, A. Nikitin, Fatigue Fract. Eng. Mater. Struct. 46 (2023) 728.

[4] G. Xue, Y. Tomoda, T. Nakamura, N. Fujimura, K. Takahashi, F. Yoshinaka, A. Takeuchi, M. Uesugi, K. Uesugi, Fatigue Fract. Eng. Mater. Struct. 45 (2022) 2693.

[5] T. Gao, H. Xue, Z. Sun, Mater. Lett. 287 (2021) 129283.

[6] H. Su, X. Liu, C. Sun, Y. Hong, Fatigue Fract. Eng. Mater. Struct. 40 (2017) 979.

[7] F. Neal, P. Blenkinsop, Acta Metall. 24 (1976) 59.

[8] X. Pan, H. Su, C. Sun, Y. Hong, Int. J. Fatigue 115 (2018) 67.

[9] X. Pan, Y. Hong, Fatigue Fract. Eng. Mater. Struct. 42 (2019) 1950.

[10] S. Heinz, D. Eifler, Int. J. Fatigue 93 (2016) 301.

[11] D. Eylon, J. Hall, Metall. Trans. A 8 (1977) 981.

[12] A. Nikitin, T. Palin-Luc, A. Shanyavskiy, Int. J. Fatigue 93 (2016) 318.

[13] X. Pan, G. Qian, S. Wu, Y. Fu, Y. Hong, Sci. Rep. 10 (2020) 4742.

[14] X. Liu, C. Sun, Y. Hong, Int. J. Fatigue 92 (2016) 434.

[15] K. Chandran, Nat Mater. 4 (2005) 303.

[16] K. Chandran, S. Jha, Acta Mater. 53 (2005) 1867.

[17] A. Nikitin, T. Palin-Luc, A. Shanyavskiy, Procedia Structural Integrity 2 (2016) 1125.

[18] C. Bathias, P. Paris, Gigacycle Fatigue in Mechanical Practice, Marcel Dekker, New York, 2005.

[19] X. Pan, S. Xu, G. Qian, A. Nikitin, A. Shanyavskiy, T. Palin-Luc, Y. Hong, Mater. Sci.

Eng. A 798 (2020) 140110.

[20]Y. Hong, X. Liu, Z. Lei, C. Sun, Int. J. Fatigue 89 (2016) 108.

[21] X. Pan, G. Qian, Y. Hong, Scripta Mater. 194 (2021) 113631.